Journal of Membrane Science & Research

journal homepage: www.msrjournal.com

Research Paper

Bubble Gas Transport Method for Binodal Distribution: Flow Rate versus Pressure Curve Splitting into Components by Modified Logistic Sigmoid Function

Alireza Chamani [1], Mohammadreza Soleimaninejad [1], Hamid Rashedi [1], Takeshi Matsuura [2, *]

[1] *Department of Chemical Engineering, College of Engineering, University of Tehran, Tehran, 1417614411, Iran*
[2] *Department of Chemical and Biological Engineering, University of Ottawa, Ottawa, Ontario, K1N 6N5, Canada*

Article info

Received 2022-11-14
Revised 2022-01-10
Accepted 2023-02-19
Available online 2023-02-19

Keywords

Pore size distribution
Bubble point gas transport method
Binodal distribution
Flow rate vs pressure curve splitting
Modified logistic sigmoid function

Highlights

- Modified logistic sigmoid function (MLSF) is applied for modeling the flow rate versus pressure curve of the bubble point gas transport method.
- For binodal pore size distribution, the experimental flow rate versus pressure curve can be split into two component pore size distributions by using MLSF.
- The binodal pore size distribution is constructed by combining the individual pore size distributions.

Graphical abstract

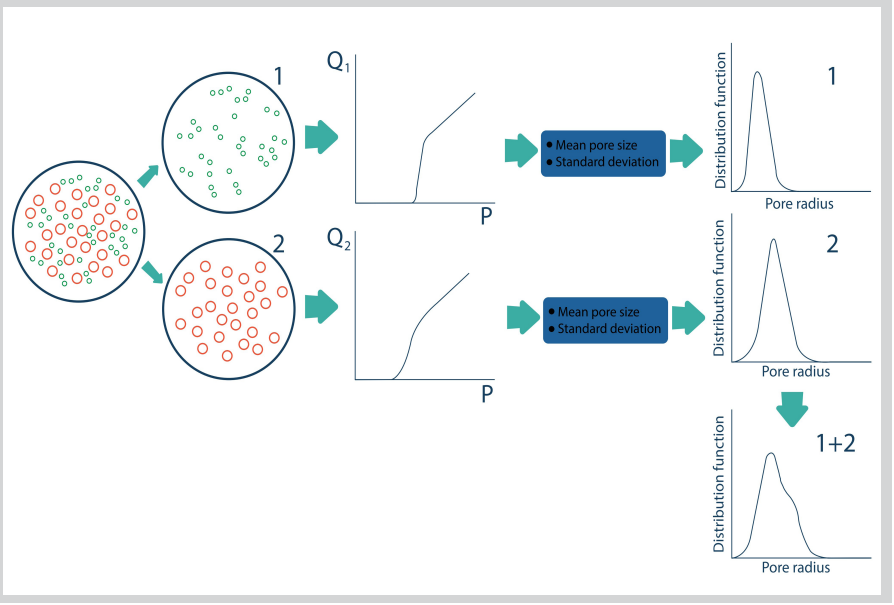

Abstract

The bubble point gas transport model is often used to determine the membrane pore size distribution due to its easiness of application. The conventional approach, in which the experimentally obtained flow rate pressure curve (hereafter called Q-P curve) is analyzed using the methods proposed by Martínez et al. and Khayat et al., is effective but becomes less accurate for the distribution of small pores. Particularly, when there are two pore size distributions, the distribution calculated for the smaller pore sizes is not very reliable. The present work challenges this problem by splitting the overall Q-P curve into two components, one from the distribution of small pores and the other from the larger pores, while modeling the Q-P curve with the modified logistic sigmoid function (MLSF). Once the overall Q-P curve is split into two components, the distribution parameters, i.e., mean pore size and standard deviations, can be obtained for each component distribution. The overall pore size distribution curve is then drawn by combining both distributions. The method is thoroughly described in this work and applied to the experimental Q-P data reported in the literature.

1. Introduction

The main purpose of membranes is to control the entry of incoming materials which can be molecules, ions, or other small particles [1,2]. Recently, membrane processes have been found as an important part of chemical technologies with various applications such as wastewater treatment,

* Corresponding author: Matsuura@uottawa.ca (T. Matsuura)

DOI: 10.22079/JMSR.2023.1973408.1577

desalination, gas and vapor separation, etc. [2]. The pore size of a membrane is one of the most significant factors governing its selectivity [3] since an inverse relationship exists between pore size and rejection. As well, there is a direct relationship between pore size and flux. Thus, membranes can be classified based on the pore size into microfiltration (MF), ultrafiltration (UF), nanofiltration (NF), and reverse osmosis (RO) membranes [4].

Both membrane users and manufacturers, as well as membrane scientists, emphasize the importance of membrane characterization in terms of pore size, pore size distribution, and solute or particle rejection efficiency for filtering membranes. The techniques used to characterize membranes by pore size and pore size distribution can be categorized into (1) approaches based on permeation and rejection performance utilizing reference molecules and particles [5], and (2) physical methods to measure the pore size and pore size distribution of a membrane. The following physical techniques are well-known for determining pore size and pore size distribution: microscopic observation, bubble pressure and gas transport, mercury porosimetry, liquid-vapor equilibrium, gas-liquid equilibrium (Permporometry), and liquid-solid equilibrium (Thermoporometry) [6]. Microscopic observation is a well-established and common method of pore size analysis [7]. Visual information on membrane morphology, such as surface pore shape and size, their distributions, pore density, surface porosity, cross-sectional structure, etc., may be obtained directly through microscopic observation and image processing of micrographs [8]. How to prepare a membrane sample without creating any errors is one of the challenges of microscopic observation [9]. Also, 2D image analyses are limited to calculating the size of surface pores and ignore the internal pores [10].

Some other ways are used to determine pore size and pore size distribution. The bubble gas transport mechanism is one of the most common methods of measuring pore size distribution. Bechhold developed the bubble gas transport method for the first time to measure the membrane's pore diameters in the early 19th century [11]. The bubble point method is another name for this approach. This technique can only determine the membrane's maximum pore size, which corresponds to the lowest pressure needed to blow the initial gas bubble [12]. The pore size distribution is measurable by combining the bubble gas transport technique with gas permeation. This combined method is called the gas bubble point extended method [12]. For the characterization of membranes, including nano-fibrous, flat sheet, and capillary and hollow fiber membranes, the bubble gas transport method and the extended method are often utilized [13]. There are also other patents related to bubble gas transport methods [14].

The method involves measuring the pressure needed to force gas through a wet membrane. The top side of a membrane is brought into contact with a liquid that seeps into all of the membrane's pores, while gas is in touch with the membrane's opposite side. The rate of flow of gas, $Q_{v,\,wet}$, increases as transmembrane pressure difference, Δp, gradually increases [15]. The $Q_{v,\,wet}$ versus Δp curve, called wet-curve (see Fig. 1) thus produced is hereafter called the Q-P curve. By considering viscous flow, Knudsen flow, or a combination of both for the gas flow mechanism in the pore, the membrane pore size distribution can be calculated. Based on this principle, several equations have been developed to calculate the pore size distribution. Among the equations, the ones developed by Martínez et al. [16] and its improved version of Khayet et al. [17], are often used for the calculation of the pore size distribution. Especially, according to the method of Khayet et al., the flow rate is also determined for the dry membrane, and it is called $Q_{v,\,dry}$ (Fig. 1).

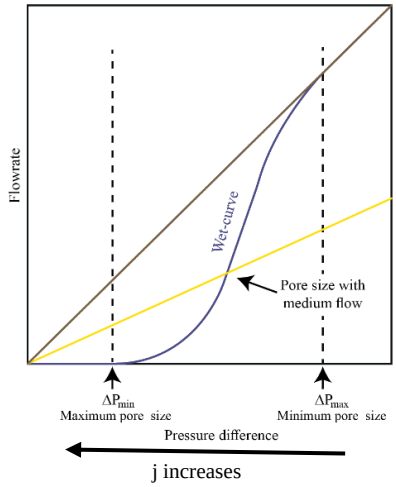

Fig. 1. Flow rate versus gas pressure (Q-P) curve obtained by the bubble gas transport method (brown line: dry-curve, blue line: wet-curve, yellow line: semi-dry (half-dry)).

The ratio of the wet and dry flow rates ($Q_{v,wet}(j)$ and, $Q_{v,dry}(j)$) through the pores that are smaller than the pore diameter $d_p(j)$ is used to define g_a function: (Note $\Delta p(j)$ decreases and $d_p(j)$ increases as j increases.)

$$g_a(j) = 1 - g'_a(j) = 1 - \frac{Q_{v,wet}(j)}{Q_{v,dry}(j)} \tag{1}$$

The incremental flow rate ratio occurring through the j[th] pore is:

$$g_d(j) = \frac{g'_a(j+1) - g'_a(j-1)}{2} \tag{2}$$

Since the flow rate through a pore is proportional to the cross-sectional area of this particular pore, the number of the j[th] pore with the diameter of $d_p(j)$ is:

$$n(j) = K\frac{g_d(j)}{d_p(j)^2} \tag{3}$$

where

$$K = \frac{g_a(n)}{\sum_{j=1}^{n}\frac{g_d(j)}{d_p(j)^2}} \tag{4}$$

and it is a constant.

And the cumulative distribution of the number of pores is:

$$n_a(j) = \sum_{k=1}^{j} n_d(k) \tag{5}$$

From Equation (1) and Fig. 1, it is obvious that both $g'_a(j-1)$ and $g'_a(j+1)$ are nearly equal to 1 when j is small, and their difference is very small, making $g_d(j)$ obtained by equation (2) susceptible to a significant error when experimental g'_as are used. The error is amplified when $n(j)$ is calculated by equation (3) for small j since $d_p(j)$ is small. Therefore, the pore size distribution calculated by the above method becomes less reliable as the pore size becomes small. This is especially true in the case of the binodal distribution where the Q-P curve for small pores appears only in the high-pressure range as shown in Fig. 2.

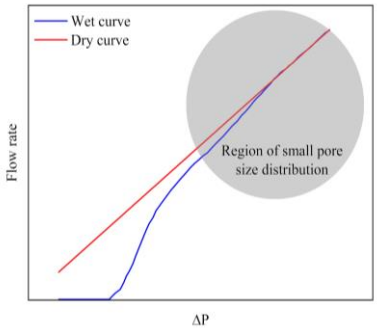

Fig. 2. Indicating the small pore region of the Q-P curve.

This problem can be solved when the overall Q-P curve is split into two component Q-P curves and the pore size distribution is calculated for each individual Q-P curve, separately.

Recently, a new method to calculate the pore size distribution was proposed [3]. This method is based on a reverse approach, i.e., firstly, a pore size distribution function is assumed and Q-P is drawn by Equation (6).

$$Q(p_n) = n_T\sum_{i=1}^{n}\left\{(CDF(r_{i-1}) - CDF(r_i))\times\frac{2}{3}\frac{\pi(\frac{2\sigma}{\frac{h}{2}+p_{i-1}})^3}{\delta\tau}(\frac{8}{\pi MRT})^{\frac{1}{2}}\right\}\times(p_{n-1}+\frac{h}{2}) +$$
$$\sum_{i=1}^{n}\left\{(CDF(r_{i-1}) - CDF(r_i))\times\frac{\pi(\frac{2\sigma}{\frac{h}{2}+p_{i-1}})^4}{16\eta g\delta\tau RT}\right\}\times(p_{n-1}+\frac{h}{2})(p_{n-1}+\frac{h}{2}+2p_e) \tag{6}$$

where $n_T(-)$ is the total number of pores. *CDF* is a cumulative distribution function, σ, *R*, *T*, τ, and δ are, respectively, surface tension, gas constant, temperature, tortuosity, and membrane thickness. Also, *r*, *p*, p_e, η_g, *h*, and *M* are pore radius, pressure at pore inlet (gauge), pressure at pore outlet (absolute), gas viscosity, pressure increment, and molecular weight, respectively. The details of the derivation of equation (6) are given in [3].

The distribution parameters, e.g., the mean pore size, μ, and the standard deviation, σ (Note σ is used for surface tension and standard deviation.), of the Gaussian normal distribution, which make the calculated Q-P curve best fit to the experimental Q-P curve, are searched for. The method enables us to find pore size distribution using fewer sets of experimental Q vs. P points. However, the method has been applied until now only for the single Gaussian distribution [3].

The pore sizes often consist of two distributions, one for the smaller pores and the other for the larger pores. Even though the larger pores are usually considered the defect pores and the number is much less than the smaller ones, their presence significantly affects the membrane's separation performance. Therefore, presenting the pore size distribution as the binodal distribution is desirable to know the membrane's separation behavior more accurately.

The objective of this work is to find a method to split the experimental Q-P curve into two components (Q-P)s, one that is for the smaller pores and the other that is for the larger pores, which is then followed by the finding of μ and σ for each component pore size distribution.

2. Methodology

As mentioned above, the wet flow rate, $Q_{v,\,wet}$, versus Δp curve (See Fig. 1) is called the Q-P curve. It should be noted that three different kinds of the Q-P curve are used in this work; i.e., 1) (Q-P)exp that is Q-P generated by the experiments, 2) (Q-P)distr that is calculated by using the Gaussian distribution parameters, μ, σ, etc. and 3) $(Q\text{-}P)_{MLSF}$ that is calculated by using the parameters involved in the modified logistic sigmoid function (MLSF), a, b, c, etc.

It was also mentioned that, according to the method proposed in [3], the two parameters of the single Gaussian pore size distribution, i.e., μ and σ are obtained by searching for the best fit (Q-P)distr to (Q-P)exp.

For the binodal distribution, one of the approaches (Approach 1) is obviously the extension of the above approach, i.e., fitting the (Q-P)distr calculated based on the binodal pore size distribution to the (Q-P)exp. It can be done by minimizing $\sum\left(Q_{binodal}-Q_{exp}\right)^2$, where $Q_{binodal}$ is the flow rate calculated based on binodal distribution and Q_{exp} is the experimental flow rate, for as many ΔP as possible. However, it was found that the convergence took a long time because there are 5 unknown parameters, i.e., μ and σ for both small (1st) and large pore size (2nd) distribution and γ (ratio of the contribution of the 2nd pore size distribution to the overall pore size distribution). Moreover, the calculation of the (Q-P)distr for a given binodal distribution is a lengthy procedure. Often, the optimization process stops before the convergence is reached.

Another approach (Approach 2) is, as suggested in the introduction, to split the (Q-P)exp into two components, $(Q\text{-}P)exp_{,1}$ that is contributed from the smaller pores and $(Q\text{-}P)exp_{,2}$ from the larger pores, followed by the finding of μ and σ for each pore size distribution.

The present work adopts Approach 2, which comprises the following steps.

Step 1. Confirm that the pore size distribution is the binodal distribution. If (Q-P)exp shows an inflection point or double peaks appear in the derivative of (Q-P)exp, it is the sign of the binodal distribution.

Step 2. The (Q-P)exp is split into two models $(Q\text{-}P)_{MLSF,1}$ and $(Q\text{-}P)_{MLSF,2}$.

For this purpose, it is assumed that the (Q-P)exp of a single distribution can be well fitted by $(Q\text{-}P)_{MLSF}$ represented by the following modified logistic sigmoid function (MLSF).

$$y=\frac{ax}{1+\exp(-(cx-b))} \tag{7}$$

where *y* and *x* represent $Q_{v,wet}$ (m^3/Nt s) and Δp (Pa), respectively, and *a*, *b*, and *c* are the fitting parameters.

Then, $(Q\text{-}P)_{MLSF}$ of the bimodal distribution can be given by

$$y=\frac{a_1x}{1+\exp(-(c_1x-b_1))}+\frac{da_2x}{1+\exp(-(c_2x-b_2))} \tag{8}$$

where a_1, b_1, c_1, a_2, b_2 and c_2 are the fitting parameters for the 1st and the 2nd distribution and *d* denotes the ratio of the contribution of the 2nd distribution to that of the 1st contribution.

The first term of equation (8) corresponds to $(Q\text{-}P)_{MLSF,1,}$ and the second term $(Q\text{-}P)_{MLSF,2.}$

Note that the model has 6 fitting parameters, i.e., a_1, b_1, c_1, da_2, b_2 and c_2. However, $y=(a_1+da_2)x$ when *x* approaches infinity. Therefore, the slope of $Q_{v,wet}$ versus Δp , which can be experimentally determined, becomes equal to a_1+da_2 at large Δp.

Thus, one of the fitting parameters is removed and 5 are left to be optimized. Even though the same number of adjustable parameters are involved in the optimization, it can go much faster than finding the optimum μ_1, σ_1, μ_2 , σ_2 and γ by Approach 1, since *y* can be calculated almost instantly for a given set of 5 unknowns chosen from a_1, b_1, c_1, da_2, b_2 and c_2.

Step 3. Generate $(Q\text{-}P)_{MLSF,1}$ using a_1, b_1 and c_1 in equation (7) and then search for μ_1 and σ_1 that will make $(Q\text{-}P)distr_{,1}$ best fit to the $(Q\text{-}P)_{MLSF,1}$, according to the method established in [3]. Similarly, μ_2 and σ_2 are found from da_2, b_2 and c_2.

Step 4. Draw the binodal pore size distribution curve.

For this purpose, γ is needed and it is obtained in the following way.

The slope of the linear portion of the (Q-P)distr should be equal to that of the $(Q\text{-}P)_{MLSF}$ when both are based on binodal distribution, but the scale of the *y*-axis of the (Q-P)distr is different from that of the $(Q\text{-}P)_{MLSF}$. Therefore,

$$\beta((1-\gamma)\alpha_1+\gamma\alpha_2)=a_1+(da_2) \tag{9}$$

where α_1 and α_2 are the slope of the $(Q\text{-}P)distr_{,1}$ and the $(Q\text{-}P)distr_{,2}$, respectively, and β is the scale ratio. (Note that γ is defined as the contribution of the 2nd distribution to the overall distribution, while *d* is defined as the ratio of the contribution of the 2nd distribution to that of the 1st distribution.)

Setting the first and the second term of the left side of equation (9) equal to those of the right side of equation (9)

$$\beta(1-\gamma)\alpha_1=a_1,\quad therefore\quad \beta=\frac{a_1}{(1-\gamma)\alpha_1} \tag{10}$$

$$\beta\gamma\alpha_2=(da_2) \tag{11}$$

From (10) and (11)

$$\frac{a_1}{(1-\gamma)\alpha_1}\gamma\alpha_2=(da_2) \tag{12}$$

Solving for γ

$$\gamma=\frac{1}{1+\frac{a_1/(da_2)}{(\alpha_1/\alpha_2)}} \tag{13}$$

The bimodal pore size distribution can be drawn, once μ_1, σ_1, μ_2 , σ_2 and γ are known.

3. Results and Discussion

3.1. Justification of the method

3.1.1. Verification of Q-P curve modeling by MLSF

To test the fitting of $(Q\text{-}P)_{MLSF}$ to (Q-P)exp, (Q-P)distr of a single Gaussian distribution is generated and used as an imaginary (Q-P)exp. Thus, (Q-P)distr is generated with $\mu=1\times10^{-6}$ and $\sigma=0.5\times10^{-6}$ m by the method described in detail in our earlier communication [3].

For this (Q-P)distr, the best-fit parameters of $(Q\text{-}P)_{MLSF}$ were found to be *a* = 1.90×10^{-17} (m^3/Nt s Pa), *b* = 6.37 and *c* = 0.70×10^{-4} (1/Pa).

Fig. 3 compares the best fit $(Q\text{-}P)_{MILF}$ with (Q-P)dist. Their agreement is excellent.

3.1.2. Fitting of Q-P curve by MLSF (Binodal Gaussian pore size distribution)

To test the fitting of $(Q\text{-}P)_{MLSF}$ (equation 8) to (Q-P)distr of the binodal Gaussian distribution, (Q-P)distr was generated with $\mu_1=1\times10^{-6}$ and $\sigma_1=0.5\times10^{-6}$ m, and $\mu_2=3\times10^{-6}$ and $\sigma_2=0.5\times10^{-6}$ m. The ratio of the contribution of the 2nd distribution to the overall distribution was 5 %. Then, the best-fit parameters for $(Q\text{-}P)_{MLSF}$ were found to be $a_1=2.26\times10^{-17}$, $b_1=6.180$, $c_1=7.63\times10^{-5}$, $da_2=2.995\times10^{-17}$, $b_2=12.88$ and $c_2=2.95\times10^{-4}$.

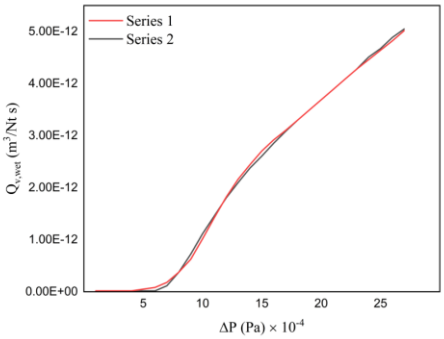

Fig. 3. Q-P curve (Series 1, (Q-P)distr generated with $\mu = 1 \times 10^{-6}$ and $\sigma = 0.5 \times 10^{-6}$ m; Series 2, the best fit $(Q\text{-}P)_{MLSF}$ with $a = 1.90 \times 10^{-13}$, $b = 6.37$ and $c = 0.70$) Note: y represents $Q_{v,wet}$ (m^3/Nt s), x is Δp (Pa) × 10^{-4}. a and c were multiplied by 10^4 because x was multiplied by 10^{-4}.

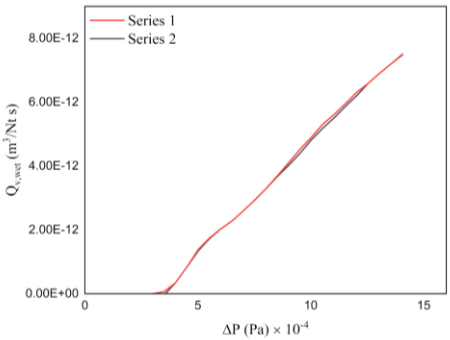

Fig. 4. Q-P curve for binodal distribution (Series 1, (Q-P)distr generated with $\mu_1 = 1 \times 10^{-6}$ and $\sigma_1 = 0.5 \times 10^{-6}$ m, and $\mu_2 = 3 \times 10^{-6}$ and $\sigma_2 = 0.5 \times 10^{-6}$ m. The ratio of the contribution of the 2nd distribution to the overall distribution was 5 %.; Series 2, the best fit $(Q\text{-}P)_{MLSF}$ with $a_1 = 2.26 \times 10^{-13}, b_1 = 6.180, c_1 = 7.63 \times 10^{-1}, da_2 = 2.995 \times 10^{-13}, b_2 = 12.88$ and $c_2 = 2.95$) Note: y represents $Q_{v,wet}$ (m^3/Nt s), x is Δp (Pa) × 10^{-4}. a and c were multiplied by 10^4 because x was multiplied by 10^{-4}.

Fig. 4 compares the best fit $(Q\text{-}P)_{MILF}$ with (Q-P)dist. The agreement is excellent.

Thus, it was proven that $(Q\text{-}P)_{dist}$ can fit $(Q\text{-}P)_{MLSF}$ very well.

3.1.3. Back-calculation of (μ_1 and σ_1) and (μ_2 and σ_2) for the 1st and 2nd pore size distribution, respectively.

Then, (μ_1 and σ_1) and (μ_2 and σ_2) for the 1st and 2nd pore size distribution, respectively, were searched for following *Step 3* of the methodology section.

The results were $\mu_1 = 1.3 \times 10^{-6}$, $\sigma_1 = 0.5 \times 10^{-6}$, $\mu_2 = 3.1 \times 10^{-6}$ and $\sigma_2 = 0.4 \times 10^{-6}$ m. The obtained mean radii and standard deviations deviated from the original ones, probably because MLSF could not fit the original Q-P curve perfectly.

3.1.4. Comparison of bimodal distribution by the proposed method with the original pore size distribution

Finally, the pore size distribution curve was drawn following *Step 4* of the methodology section.

By drawing $(Q\text{-}P)distr_{,1}$ using $\mu_1 = 1.3 \times 10^{-6}$ and $\sigma_1 = 0.5 \times 10^{-6}$, α_1 is found to be 3.88×10^{-17}. Similarly, by drawing $(Q\text{-}P)distr_{,2}$, using $\mu_2 = 3.1 \times 10^{-6}$ and $\sigma_2 = 0.4 \times 10^{-6}$, α_2 is found to be 6.04×10^{-16}. Then, using $a_1 = 2.26 \times 10^{-17}$ and $da_2 = 2.995 \times 10^{-17}$ in equation (13), $\gamma = 0.0785$.

The binodal pore size distribution so obtained from the fitted MLSF model is shown in Fig. 5a and compared with the original binodal distribution (Fig. 5b).

The fitted MLSF model shows a slightly higher peak for the second distribution.

3.2. Analysis of the experimental data in the literature

The papers in which the experimental Q-P curve ((Q-P)exp) for the binodal distribution is reported together with the pore size distribution are scarce in the literature. One of those is the paper by Peinador et al. [18] who reported the (Q-P)exp for cotton fiber face mask (FM) and cellulose nitrate membrane (CN), and determined the binodal pore size distribution by Gas Liquid Displacement Porometry (GLDP). They used water (surface tension 72.0 mN/m) and commercial liquid Fluorinert FC-43 (surface tension 16.0 mN/m) as the liquid phase, for FM and CN, respectively.

Applying *Step 2* of the method section to their (Q-P)exp data, the best fit MLSF parameters were obtained for both FM and CN, and the results are shown in the 2nd and 3rd columns of Table 1.

Fig. 6 shows the curves for (Q-P)exp reported by Peinador et al. and $(Q\text{-}P)_{MLSF}$ calculated with the above MLSFs parameters.

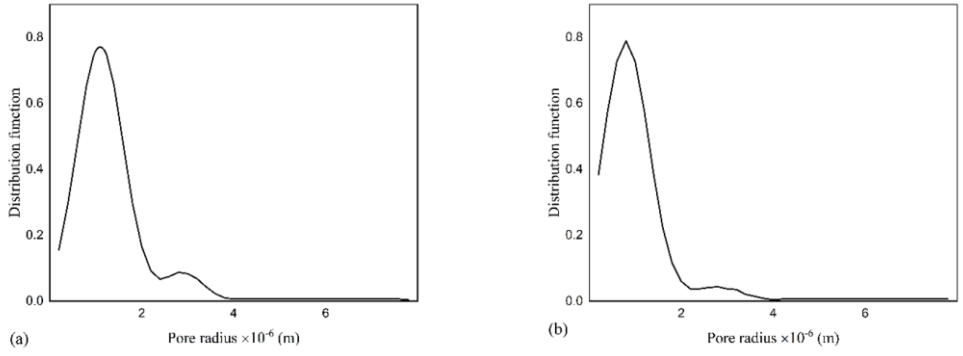

Fig. 5. a) Binodal pore size distribution obtained from the fitted MLSF model, b) Original binodal distribution.

Table 1
MLSF and pore size distribution parameters for the cotton fiber face mask (FM) and cellulose nitrate membrane (CN).

	MLSF parameters		Pore size distribution parameters		
	a_1, b_1, c_1	da_2, b_2, c_2	μ_1, σ_1	μ_2, σ_2	γ^a
Face mask (FM)	$a_1 = 14459$ $b_1 = 41.65$ $c_1 = 235 \times 10^{-5}$	$da_2 = 66191$ $b_2 = 12.0$ $c_2 = 78.3 \times 10^{-5}$	$\mu_1 = 8.37$ µm $\sigma_1 = 0.37$ µm	$\mu_2 = 8.5$ µm $\sigma_2 = 1.5$ µm	0.757
Cellulose nitrate membrane (CN)	$a_1 = 490$ $b_1 = 316.2$ $c_1 = 1209 \times 10^{-5}$	$da_2 = 59025$ $b_2 = 13.08$ $c_2 = 64.99 \times 10^{-5}$	$\mu_1 = 1.23$ µm $\sigma_1 = 0.018$ µm	$\mu_2 = 1.5$ µm $\sigma_2 = 0.2$ µm	0.99177

γ^a is the contribution of the second pore size distribution.

Note that $(Q\text{-}P)_{MLSF}$ can represent (Q-P)exp very well for both FM and CN, indicating that the MLSF parameters were well chosen. In particular, the agreement of $(Q\text{-}P)_{MLSF}$ with (Q-P)exp is so good for CN that the $(Q\text{-}P)_{MLSF}$ line covers completely that for (Q-P)exp (Fig. 6b). It is also noted that the first inflection point appears at about 0.17×10^5 Pa and the second one at about 0.25×10^5 Pa in the Q-P curve of FM. On the other hand, one inflection point appears at about 0.21×10^5 Pa but no obvious second inflection point is seen in the Q-P curve of CN.

Then, following *Step 3* of the method section,(μ_1 and σ_1) and (μ_2 and σ_2) were obtained for both FM and CN. Those values are listed in the 4th and 5th columns of Table 1.

Finally, following *Step 4* of the method section, the pore size distribution was generated for both FM and CN, and the results are shown in Figs. 7a and b, respectively.

Fig. 7a shows a peak at about 8×10^{-6} m with a broad tailing thereafter, reflecting the large contribution ($\gamma = 0.757$) of the second peak. Fig. 7b shows an almost symmetrical peak with a mean pore radius of 1.5×10^{-6} m. This is the second peak whose contribution is so large ($\gamma = 0.9917$) that the first peak shows practically no contribution.

The pore size distributions reported by Peinador et al. are shown in Figs. 8a and b. Note that the y-axis of Figs. 8a and b is permeability, while the y-axis of Figs. 7a and b is 1/m. (Most likely, the distribution in Fig. 8 is based on the pore area while the distribution in Fig. 7 is based on the pore number.) Therefore, Figs. 7 and 8 do not correspond to each other directly. Nevertheless, we are allowed to compare the shapes of the distribution curves given in Figs. 7 and 8.

Comparing Fig. 7a and Fig. 8a, both figures have a sharp peak at around 8×10^{-6} m, which is the first peak. Both have the tailing contributed by the second peak. But the second peak is more pronounced in Fig. 7a due to its high γ value. In other words, the first peak contributes less to the entire pore size distribution in Fig. 7a than in Fig. 8a.

Comparing Figs.7b and 8b, both figures have a peak at 1.5×10^{-6} m, which in this case is the second peak. Fig. 7b is symmetrical around the mean radius due to its very large γ value ($\gamma = 0.9917$). As for Fig. 8b, a small peak appears at around 1.2×10^{-6} m, which seems to be the contribution of the first peak. In fact, no inflection point appears in Fig. 6b in the high range of Δp. Therefore, the appearance of the peak in the small range of the pore radius seems unreasonable.

In any case, for both FM and CN, the newly proposed method leads to less contribution of the 1st smaller pore sizes than what the GLDP machine shows.

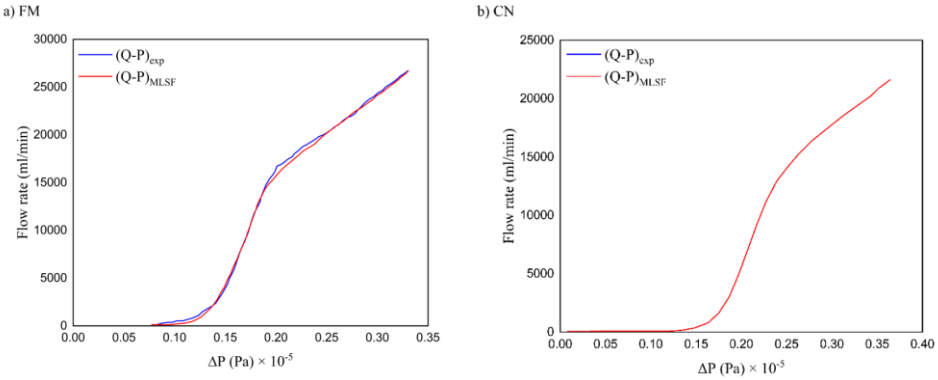

Fig. 6. Comparison of $(Q\text{-}P)_{MLSF}$ with (Q-P)exp a) for FM, b) for CN (Blue, (Q-P)exp by Peinador et al. [18]; Red, $(Q\text{-}P)_{MLSF}$).

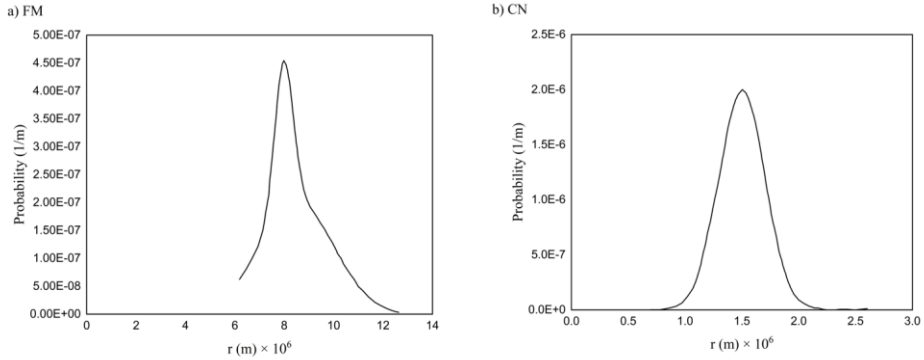

Fig. 7. Pore size distribution obtained by the proposed method from the experimental data of Peinador et al. [18] a) for FM, b) for CN.

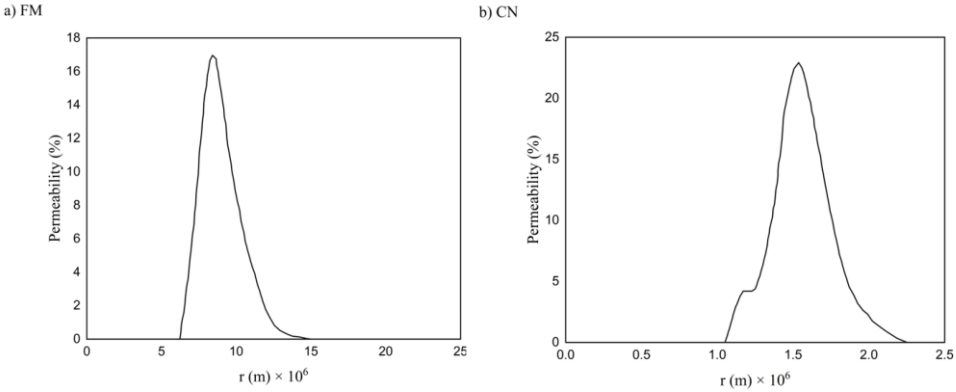

Fig. 8. Pore size distribution determined by GLDP a) FM, b) CN (redrawn from Fig. 7 of Peinadar et al. [18]).

4. Conclusions

From this work, the following conclusions can be drawn.

1. MLSF can be used for modeling the experimental Q-P curve of the bubble point gas transport method.
2. The overall Q-P curve can be split into its component curves, one contributed from the small pore size distribution and the other large pore size distribution by the aid of MLSF as the model equation.
3. The mean pore size and the standard deviation of each pore size distribution can be obtained from each component Q-P curve generated with the aid of MLSF.
4. The method is applicable to obtain binodal distribution parameters for the experimental Q-P curve taken from the literature.

The following future work is suggested.

1. Apply the polynomial function to improve the modeling of the Q-P curve.
2. Apply another method such as the Bézier curve method to improve the modeling of the Q-P curve.

Credit authorship contribution statement

A. Chamani: Data curation; Formal analysis; Validation; Visualization; Writing – original draft.
M. Soleimaninejad: Data curation; Formal analysis; Visualization; Writing – original draft.
H. Rashedi: Supervision.
T. Matsuura: Supervision; Methodology; Writing – review & editing.

Funding sources

This research did not receive any specific grant from funding agencies in the public, commercial, or not-for-profit sectors**.**

Declaration of Competing Interest

The authors declare that they have no known competing financial interests or personal relationships that could have appeared to influence the work reported in this paper.

References

[1] M. Mulder, Basic Principles of Membrane Technology, 2nd Ed., Kluwer Academic Publishers. Boston, MA. 1996. https://doi.org/10.1007/978-94-009-1766-8.
[2] R.W. Baker, Membrane Technology and Applications, 3rd Ed, Wiley, New York, 2012. https://doi.org/10.1002/9781118359686.
[3] H. Chamani, T. Matsuura, D. Rana, CQ. Lan, A reverse approach to evaluate membrane pore size distribution by the bubble gas transport method using fewer experimental data points, Desalination 518 (2021) 115287. https://doi.org/10.1016/j.desal.2021.115287.
[4] C. Charcosset, Ultrafiltration, microfiltration, nanofiltration, and reverse osmosis in integrated membrane processes, in: A. Basile, C. Charcosset, Integrated membrane systems and processes, 2016. https://doi.org/10.1002/9781118739167.ch1.
[5] H. Guo, X. Xu, J. Li, W. Feng, M. Zhang, C. Fang, L. Zhu, Chemically tailored microporous nanocomposite membranes with multi-channels for intensified solvent permeation, J. Membr. Sci. 660 (2022) 120877. https://doi.org/10.1016/j.memsci.2022.120877.
[6] S.I. Nakao, Determination of pore size and pore size distribution: 3. Filtration membranes, J. Membr. Sci. 96 (1994) 131-165. https://doi.org/10.1016/0376-7388(94)00128-6.
[7] J.R. Nimmo, Porosity and pore size distribution, in: D. Hillel, Encyclopedia of Soils in the Environment, Elsevier, 2004. https://doi.org/10.1016/b0-12-348530-4/00404-5.
[8] R.H. Gong, A. Newton, Image-analysis techniques, J. Text. Inst. 83 (1992) 253-268. https://doi.org/10.1080/00405009208631195.
[9] C. Zhao, X. Zhao, Y. Yue Determination of pore size and pore size distribution on the surface of hollow-fiber filtration membranes: a review of methods, Desalination 129 (2000) 107-123. https://doi.org/10.1016/S0011-9164(00)00054-0.
[10] F.A. AlMarzooqi, M.R. Bilad, B. Mansoor, H.A. Arafat, A comparative study of image analysis and porometry techniques for characterization of porous membranes, J. Mater. Sci. 51 (2016) 2017-2032.. https://doi.org/10.1007/s10853-015-9512-0.
[11] F.P. Cuperus, C.A. Smolders, Characterization of UF membranes: membrane characteristics and characterization techniques, Adv. in Colloid Interface Sci. 34 (1991) 135-173. https://doi.org/10.1016/0376-7388(91)80007-s.
[12] A.C. Hernández, J.I. Calvo, P. Prádanos, F. Tejerina, Pore size distributions in microporous membranes, J. Membr. Sci. 112 (1996) 1-12.https://doi.org/10.1016/0376-7388(95)00025-9.
[13] R. Gopal, S. Kaur, Z. Ma, C. Chan, S. Ramakrishna, T. Matsuura, Electrospun nanofibrous filtration membrane, J. Membr. Sci. 281 (2006) 581-586. https://doi.org/10.1016/j.memsci.2006.04.026.
[14] G. Reichelt, Method for determining the bubble point or the largest pore of membranes or of filter materials. *United States Patent No. US0053485*, 1988.
[15] I.G. Wenten, K. Khoiruddin, A.N. Hakim, N.F. Himma, The bubble gas transport method,in: N. Hilal, A. Fauzi Islami, T. Matsuura, D. Oatley-Radcliffe, Membrane Characterization, Elsevier, 2017, pp. 199-218. https://doi.org/10.1016/B978-0-444-63776-5.00011-5.
[16] L. Martínez, F.J Florido- Díaz, A. Hernández, P. Prádanos, Characterisation of three hydrophobic porous membranes used in membrane distillation: Modelling and evaluation of their water vapour permeabilities, J. Membr. Sci. 203 (2002) 15-27.https://doi.org/10.1016/S0376-7388(01)00719-0.
[17] M. Khayet, A. Velázquez, J.I. Mengual, Modelling mass transport through a porous partition: effect of pore size distribution, J. Non-Equilib. Thermodyn. 29 (2004) 279-299. https://doi.org/10.1515/JNETDY.2004.055.
[18] R.I. Peinador, I. José, J.I. Calvo, R. Ben Aim, Comparison of capillary flow porometry (CFP) and liquid extrusion porometry (LEP) techniques for the characterization of porous and face mask membranes, Appl. Sci. 10 (2020) 5703.. https://doi.org/10.3390/app10165703.